Performance limit of a multi-frequency probe based coherent optical time domain reflectometry caused by nonlinear effects

Lidong Lü (吕立冬), Yuejiang Song (宋跃江), Fan Zhu (朱 帆), and Xuping Zhang (张旭苹)*

Institute of Optical Communication Engineering, Nanjing University, Nanjing 210093, China

**Corresponding author: xpzhang@nju.edu.cn*

Received August 30, 2011; accept October 25, 2011; posted online January 13, 2012

The nonlinear effects that limit the performance of the multi-frequency probe (MFP) based coherent optical time domain reflectometry (C-OTDR) are investigated. Based on theoretical analysis and experimental results, compared with conventional C-OTDR, when the probe pulse has power gradient within the pulse width, self-phase modulation (SPM) and cross-phase modulation (XPM) are strengthened in the new C-OTDR scheme. The generation of four-wave mixing (FWM) is dependent on SPM and XPM, and with modulation frequency of phase modulator higher than 40 MHz, the stimulated Brillouin scattering (SBS) threshold can be enhanced by more than 5 dB, which benefits the maximum dynamic range of the MFP C-OTDR.

OCIS codes: 060.2370, 120.4825.

doi: 10.3788/COL201210.040604.

Coherent optical time domain reflectometry (C-OTDR) is a commonly used instrument for fiber characterization and fault location for long-haul multi-fiber span optical transmission line monitoring[1,2]. At present C-OTDR is the sole instrument for super long undersea optical transmission line monitoring. Generally, the transmission line is thousands of kilometers in length with multiple fiber spans and repeaters of erbium-doped fiber amplifier (EDFA), and it may take several hours to perform a successful measurement for such long transmission line.

The monitoring schematic diagram is shown in Fig. 1. Since conventional C-OTDR is based on a single-frequency probe, it only obtains one intermediate frequency (IF) by coherent detection[3]. In this letter, we use a phase modulator (PM) to convert a single-frequency probe to multiple frequencies and keep the local oscillator (LO) as the original single frequency. Afterwards, we can simultaneously detect and process multiple IF signals generated in the coherent detection process between the Rayleigh signals of the multi-frequency probe backscattered in the fiber under test (FUT) and the original single-frequency LO. This process speeds up measurement efficiency, compared with conventional single-frequency probe based C-OTDR[4,5].

The schematic diagram of the multi-frequency probe (MFP) based C-OTDR is shown in Fig. 2. External cavity laser diode (ECLD) with a narrow linewidth of 3.7-kHz generates light with a wavelength of 1 561.42 nm. The laser output from ECLD was split into two paths by a 90/10 coupler. The one with higher power was used for probe light, and the other was used as LO. The state of polarization (SOP) of the probe light was adjusted to minimize the insertion loss of PM. The modulation depth of PM was fixed at 1.44, so the output power of PM was concentrated on three frequencies (0 and ±1 order), all of which had the same light power[6]. The multi-frequency probe light power was adjusted by variable optical attenuator (VOA) to make each of the three frequencies have the same power level with the condition of single-frequency probe light interaction in order to conduct performance comparison of the two methods. The probe pulses were generated by acousto-optic modulator (AOM) and polarization scrambled using a polarization scrambler (PS). Then, they were launched into the first port of the circulator and into the FUT through the second port of the circulator. The FUT was combined using two fiber sections. Finally, backscattered Rayleigh light output from the third port of the circulator was combined with LO in a 3-dB coupler. Coherent heterodyne generated many IF signals, which were detected by a balanced photo detector (BPD); meanwhile, only three IF signals corresponding to the probe were filtered out for processing using the band pass filters (BPFs) of the corresponding pass channels with a bandwidth of 1 MHz[7]. Since C-OTDR is mainly used in long-range multi-fiber span undersea optical transmission line monitoring, in this application situation, accumulated amplified spontaneous

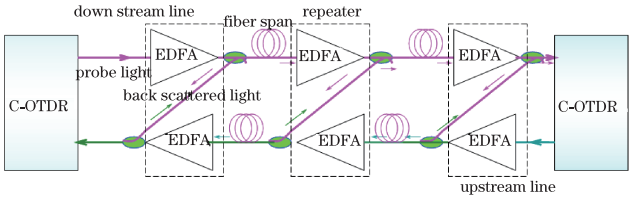

Fig. 1. Schematic diagram of C-OTDR measurement for long-haul multi-fiber span undersea optical fiber transmission line.

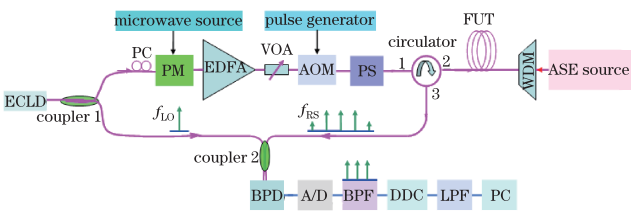

Fig. 2. Experimental system configuration of the MFP C-OTDR. DDC: digital down conversion; LPF: low pass filter.

emission (ASE) noise is dominant over thermal noise and shot noise; therefore, the beat noise between ASE noise and LO becomes dominant in the noise term of signal-to-noise ratio (SNR). As such, we used the ASE source and a wavelength division multiplexer (WDM) with a center wavelength of 1 561.42 nm, and a 3-dB bandwidth of 0.6 nm to obtain effective ASE disturbance from the fiber end[2]. The ASE power intensity was set at –8 dBm/nm.

When the PM was turned off, it became a conventional single-frequency probe based C-OTDR. Figure 3 illustrates the OTDR traces obtained by conventional C-OTDR and MFP C-OTDR. Both OTDR traces are the average of 2^{18} measurements. Compared with the conventional single-frequency probe based C-OTDR, MFP COTDR can obtain triple measurement numbers in the same measurement time, bringing a much lower OTDR trace fluctuation and a 2.4-dB dynamic range enhancement, as shown in Fig. 3. Testing results demonstrate that the measurement efficiency of MFP C-OTDR is nearly triple that of conventional C-OTDR. Therefore, using the proposed MFP C-OTDR scheme saves time in conducting super long optical transmission line monitoring.

Self-phase modulation (SPM), cross-phase modulation (XPM), four-wave mixing (FWM), and stimulated Brillouin scattering (SBS) are the main nonlinear effects that may exist in the C-OTDR system and limit its performance. Detailed research on this issue in conventional C-OTDR has been described in Ref. [8]. For MFP C-OTDR, as the multi-frequency probe is converted from single-frequency light by PM, multi-frequencies co-propagate in the FUT, which brings new changes in nonlinear effect interaction process compared with conventional C-OTDR. For comprehensive evaluation of our MFP C-OTDR, we analyzed and discussed the nonlinear effects that limit the performance of C-OTDR.

The direct consequence caused by nonlinear effects on the multi-frequency probe light is the reconfiguration of light frequency and power. Thus, we should first know the power spectrum of multi-frequency probe light generated by PM, and then investigate the changes brought about by the nonlinear effects. When light with angular frequency of ω passes through PM, it is converted to multi-frequency light with equal frequency separation[6]. It can be expressed as

$$E = \sqrt{P_0}\exp(\mathrm{j}\omega t)\sum_{q=-\infty}^{\infty} J_q(A_\mathrm{m})\exp(\mathrm{j}q\omega_\mathrm{m}t), \quad (1)$$

where $\sqrt{P_0}$ is the amplitude of the output light from PM; ω is the original angular frequency of the input light;

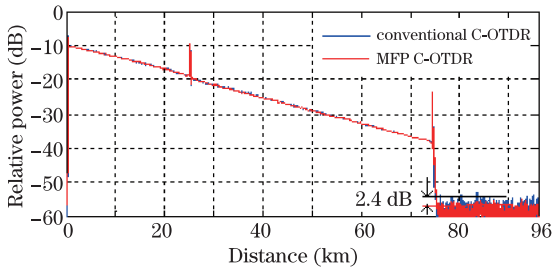

Fig. 3. OTDR trace comparison of two C-OTDR schemes.

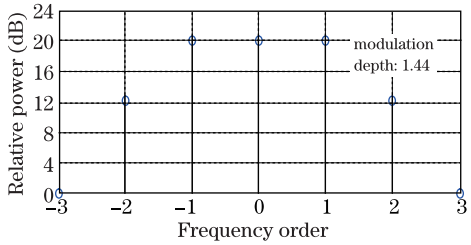

Fig. 4. Theoretical power spectrum of the multi-frequency light generated by PM.

ω_m and A_m are the modulation angular frequency and modulation depth of the PM, respectively; q is the frequency order of the multi-frequency light with a value of 0, ±1, ±2. When the modulation depth is 1.44, three frequencies (0, ±1 orders) have the same magnitude, each taking up 30% of the total output light power. The power spectrum of the multi-frequency light is shown in Fig. 4 and five frequency orders, namely, 0, ±1, and ±2 contain 99.94% of the total light power.

Both SPM and XPM are induced by the optical Kerr effect. Thus, the variation of the non-linear refractive index of the fiber is dependent on light power propagating in it; in turn, this leads to the non-linear phase shift $\Delta\phi_\mathrm{NL}$ of the propagating light[9]. The variation of nonlinear refractive index caused by the optical Kerr effect of the multi-frequency light co-propagating in fiber can be expressed as

$$\Delta n_j^\mathrm{NL} \approx \varepsilon_j^\mathrm{NL}/2n_j \approx \sum_{j,k=-q,j\neq k}^{q} n_2(|E_j|^2 + 2|E_k|^2), \quad (2)$$

where n_2 is the nonlinear refractive index coefficient, and q and E_q are the frequency order and amplitude of the multi-frequency light, respectively. The first term on the right of Eq. (2) is related to SPM, and the second term is related to XPM. Therefore, in the same condition, XPM contributes to double nonlinear refractive index compared with SPM. When the PM modulation frequency is 1.44, the power of the multi-frequency light is concentrated on three dominant frequencies—0, ±1 orders—as shown in Fig. 4. The contribution to the nonlinear refractive index by other frequency orders can be omitted due to their much lower power level. Then, the nonlinear phase shift can be written as

$$\phi_j^\mathrm{NL}(z) = \frac{\omega_j z}{c}\Delta n_j^\mathrm{NL} = \frac{\omega_j z n_2}{c}\sum_{j,k=-1,j\neq k}^{1}(|E_j|^2 + 2|E_k|^2)$$

$$= \frac{\omega_j z n_2}{c}\sum_{j,k=-1,j\neq k}^{1}(P_j + 2P_k). \quad (3)$$

The temporal derivative of the nonlinear phase shift $\Delta\phi_\mathrm{NL}$ causes frequency change Δf of the propagating light, which is also proportional to the temporal derivative of power[8,9]. It can be expressed as

$$\Delta f = \frac{\partial\phi_j^\mathrm{NL}(t)}{\partial t} = \frac{\omega_j z n_2}{c}\frac{\partial P(t)}{\partial t}, \quad (4)$$

where $P(t) = \sum_{j,k=-1,j\neq k}^{1}(P_j + 2P_k)$, c is light velocity in vacuum, ω_j is the angular frequency of the jth order,

n_2 is nonlinear refractive index coefficient, and $z = v_g t$. According to Eq. (4), for probe pulse propagating in the fiber, when the probe pulse generated by AOM has a power gradient within the pulse width of t, it can lead to the frequency shift of the propagating light. Once the frequency shift exceeds the bandwidth range of the corresponding BPF[8], it degrades the OTDR trace as a result of the power loss of the backscattered Rayleigh signals. Additionally, each frequency contributes to the frequency shift Δf; thus, in MFP C-OTDR, the SPM and XPM are strengthened, and it triples the frequency shift Δf in the same probe pulse waveform, compared with the single-frequency probe light. Therefore, to suppress SPM and XPM, the best approach is to use high performance AOM to generate power flatness probe pulse.

FWM is a parameter interaction process of multiple waves generating new waves. For FWM, the most significant condition is phase matching among the propagating light. The phase matching condition can be expressed as[9,10]

$$\begin{aligned}\Delta k &= k_i + k_j - k_l - k_m \\ &= (n_i\omega_i + n_j\omega_j - n_l\omega_l - n_m\omega_m)/c, \end{aligned} \tag{5}$$

where Δk is the phase mismatching number; k_i and k_j are arbitrary two wave vectors of the multi-frequency light, respectively; k_l and k_m are the wave vectors of the newly generated waves by FWM, respectively. In addition, $n_{q=i,j,l,m}$ and $\omega_{q=i,j,l,m}$ are the refractive index and angular frequency of the corresponding wave, respectively. Only when $\Delta k = 0$ is satisfied can FWM appear. Based on Eqs. (1) and (2), we can obtain the following relationships of the multi-frequency light generated by PM with modulation depth of 1.44:

$$n_{q=i,j,l,m} = n^{\mathrm{L}} + \Delta n_x^{\mathrm{NL}}, \tag{6}$$

$$\Delta n_{-2}^{\mathrm{NL}} = \Delta n_2^{\mathrm{NL}} \neq \Delta n_0^{\mathrm{NL}} = \Delta n_{-1}^{\mathrm{NL}} = \Delta n_1^{\mathrm{NL}}, \tag{7}$$

where n^{L} is the linear refractive index. Since the frequency separation of the multi-frequency light is relatively low, their linear refractive indexes for all the frequencies are the same. Based on the power spectra of the multi-frequency light shown in Fig. 4 and Eqs. (5) and (7), it is difficult to satisfy the phase matching condition due to the mismatching refractive indexes of the interaction waves. Figure 5 shows the power spectrum of the multi-frequency light after propagating in a 75-km fiber delay line, which well fits the theoretical computation shown in Fig. 4. The power spectrum is obtained by heterodyne method, and the multi-frequency light has a 40-MHz frequency shift by AOM before launching into the 75-km fiber delay line. Thus, the 0-order frequency appears at a 40-MHz position, and other frequency orders are symmetrically distributed on both sides.

A common way to satisfy the phase matching condition as described in Eq. (5) is to change the frequency of the co-propagating light by SPM and XPM. For probe pulse, FWM generation is strongly dependent on SPM and XPM. As presented by Izumita *et al.*[8] using a probe pulse width of 100 ns resulted in the appearance of the FWM, which limited the incident probe power. This is because the total rise time and fall time of AOM may

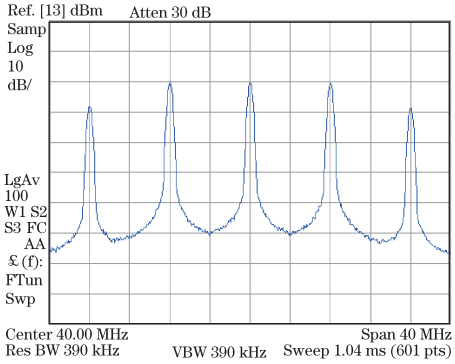

Fig. 5. Power spectrum of the multi-frequency light after propagating in a 75-km fiber.

exceed 40 ns[8,11,12] in such short pulse width range. In turn, this leads to drastic SPM and XPM for large power gradient existing in the pulse width, which induces FWM as the result of satisfying the phase matching condition. Based on the above analysis and discussion, we conclude that for the multi-frequency probe in MFP C-OTDR, generation of FWM depends on SPM and XPM.

SBS is a main barrier that limits the dynamic range enhancement of C-OTDR[8]. When the probe power reaches the SBS threshold, much of its energy can transfer to the SBS spectra. Further improving the probe power, the received power of backscattered Rayleigh signals does not increase or even reduce. Thus, it is very important to find a good way to suppress SBS and effectively increase probe light power. PM is an excellent choice, which is widely used in lightwave cable television (CATV) systems for SBS suppression[13,14]. In our new C-OTDR scheme, PM plays important roles in generating multi-frequency light and suppressing SBS to obtain the maximum dynamic range. In order to obtain the maximum dynamic range, we investigated the SBS threshold improvement effect by PM with a modulation depth of 1.44. Therefore, we conducted corresponding experiments. The experimental schematic diagram is shown in Fig. 6. The SBS threshold measurement method has been described previously in Ref. [13]. We used a VOA to gradually increase the power of the multi-frequency light generated by PM until it became much higher than SBS threshold. When the light power reached or exceeded the SBS threshold, the output power from the fiber end became a relatively stable value with weak fluctuation.

The experimental testing results are shown in Fig. 7, which shows that the output light of our ECLD has a SBS threshold of 7.0 dBm; moreover, when the modulation frequency is higher than 40 MHz, the SBS threshold is improved by more than 5 dB. Low PM modulation frequency cannot improve SBS threshold, because once modulation frequency is lower than the bandwidth of the SBS gain spectrum, the gain spectra of the multi-frequency light begin to overlap, thereby degrading the SBS suppression capability[14]. Therefore, in order to obtain the maximum dynamic range, it is necessary to improve the modulation frequency of PM.

When PM modulation depth is 1.44, each power of the three dominant frequencies is 5.2 dB lower than that before modulation[6]; thus, increasing multi-frequency light power by 5.2 means that each of the three dominant

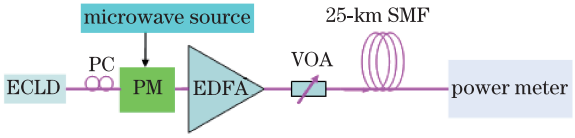

Fig. 6. Experimental setup for the SBS threshold measurement.

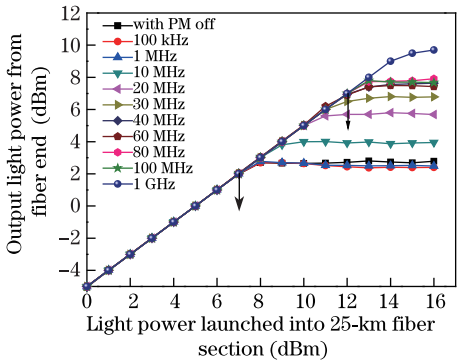

Fig. 7. SBS threshold measurement in different PM modulation frequencies, with PM modulation depth of 1.44.

frequencies equals the single-frequency light before the power increase. Therefore, compared with the conventional single-frequency probe based C-OTDR, according to the experimental results shown in Fig. 7, SBS threshold improvement by PM in the MFP C-OTDR cannot enhance the maximum dynamic range; in addition, the dynamic range is improved mainly by enhancing measurement efficiency[4,5].

In conclusion, the non linear effects that limit the performance of the MFP C-OTDR are investigated and discussed. Theoretical analysis and experimental results illustrate that SPM, XPM, and FWM are strongly dependent on the probe pulse quality generated by AOM. Compared with conventional probes based on a single frequency, when the probe pulse has power gradient within its pulse width, these nonlinear effects can become much stronger; in turn, generation of FWM depends on SPM and XPM in order to satisfy the phase matching condition. With a PM modulation depth of 1.44 and a modulation frequency higher than 40 MHz, the SBS threshold of the multi-frequency light can be improved by more than 5 dB. Comparison of the maximum dynamic range between conventional C-OTDR and the MFP C-OTDR shows that using the new C-OTDR scheme to improve SBS cannot greatly increase maximum dynamic range; instead, the enhancement of dynamic range is caused by the rapid reduction of noise level than that observed in the conventional C-OTDR. This is because its measurement efficiency is triple that of the conventional C-OTDR.

This work was supported by the National "973" Program of China (No. 2010CB327803) and the National Natural Science Foundation of China (Nos. 61027617, 60907022, and 60644001).

References

1. S. Furukawa, K. Tanaka, Y. Koyamada, and M. Sumida, IEEE Photon. Technol. Lett. **7,** 540 (1995).
2. Z. Feng, S. Qiu, Y. Wei, L. Li, G. N. Liu, and Q. Xiong, in *Proceedings of ACP2009* WL86 (2009).
3. J. P. King, D. F. Smith, K. Richards, P. Timson, R. E. Epworth, and S. Wright, J. Lightwave Technol. **5,** 616 (1987).
4. M. Sumida, IEEE Photon. Technol. Lett. **7,** 336 (1995).
5. M. Sumida, J. Lightwave Technol. **14,** 2483 (1996).
6. F. W. Willems and J. S. Leong, IEEE Photon. Technol. Lett. **6,** 1476 (1994).
7. S. Furukawa, K. Tanaka, and Y. Koyamada, in *Proceedings of IMTC 94* TUPM5-2 (1994).
8. H. Izumita, Y. Koyamata, S. Furukawa, and I. Sankawa, J. Lightwave Technol. **12,** 1230 (1994).
9. G. Agrawal, Nonlinear Fiber Optics (Academic Press, San Diego, 2001).
10. Z. Wang, Y. Fu, Y. Song, G. Dai, F. Wen, J. Zhao, and Y. Zhang, Chin. Opt. Lett. **9,** 072701 (2011).
11. H. Izumita, Y. Koyamada, S. Furukawa, and I. Sankawa, J. Lightwave Technol. **15,** 267 (1997).
12. K. Shimizu, T. Horiguchi, and Y. Koyamada, J. Lightwave Technol. **10,** 982 (1992).
13. J. Yang, Z. Guo, and K. Zha, Chinese J. Lasers (in Chinese) **28,** 439 (2001).
14. W. Chen and M. Zhou, Chinese J. Lasers (in Chinese) **38,** 0305002 (2011).